Dose in media equivalent to bone and lung for 6 and 15 MV photon beams

Author: Neus Miquel i Armengol
*Facultat de Física, Universitat de Barcelona, Diagonal 645, ES-08028 Barcelona, Catalonia**

Advisor: Dr. José M. Fernández-Varea

Abstract: In this project we studied the behaviour of calculation algorithms used for planning radiotherapy treatments in heterogeneous media. The work consisted in measuring the absolute absorbed dose with an ionization chamber inside media equivalent to lung and bone for 6 and 15 MV photon beams. The measurements were compared to Monte Carlo simulations done with the PENELOPE/penEasy code and to the calculations of the AAA and Acuros algorithms.

I. INTRODUCTION

Radiotherapy is a modality of oncological treatment that employs ionizing radiation to eliminate cancer cells; it is normally used to complement surgery and/or chemotherapy in order to achieve complete tumour control. The radiotherapy treatment must be planned very precisely to obtain the desired dose distribution in the patient, delimiting accurately the volume around the tumour to be irradiated and avoiding radiosensitive organs.

When a photon (x-ray) beam is emitted from the linear accelerator (linac), it penetrates the patient traversing different tissues before reaching the tumour. The planning system must incorporate very effective calculation algorithms in order to optimize the treatment plan and finalize it within an hour or so, to be able to treat a large number of patients per year. CPU time is, therefore, a key factor. Moreover, differences between calculations and measurements must be at most 2%. This has led to the continued development of new algorithms, improving their accuracy with respect to the preceding ones and taking advantage of the available computational tools.

Recently, the marketing of a new calculation algorithm called Acuros for radiation therapy with megavoltage x-ray beams has begun. In this project we wanted to quantify the improvement that this algorithm introduces in the calculation of absorbed dose. To this end we have compared the absolute dose calculated by Acuros and the older AAA (Anisotropic Analytical Algorithm) using phantoms made of plastic water containing slabs of bone- and lung-equivalent materials, with measurements and Monte Carlo simulations.

II. MATERIALS AND METHODS

A. Experimental measurements

The experimental data were taken at the Hospital de la Santa Creu i Sant Pau during the internship period. A Varian Clinac 2100 C/D accelerator was used to deliver 6 and 15 MV beams than impinged on various phantoms. The field size on the phantom surface was always 10 cm × 10 cm as delimited by the primary and secondary collimators of the linac, and the source-to-surface distance was 100 cm.

The phantoms were $30 \times 30 \times 15$ cm^3 paralellepipeds made stacking three 5-cm-thick layers. The top and bottom ones were plastic water and the central slab could also be plastic water or either lung- or bone-equivalent material, see Fig. 1.

FIG. 1: Homogeneous phantom of water-equivalent material (left) and heterogeneous phantom including a layer of lung-equivalent material (right).

To obtain the dose under reference conditions we employed a cylindrical ionization chamber PTW 30013 coupled to a Inovision 35040 electrometer and a plastic water phantom (whose photon-interaction properties for MV beams are practically the same as liquid water) irradiated with 100 MU (Monitor Units). MU is a measure of a machine output; generally, a monitor chamber reads 100 MU when an absorbed dose of 1 Gy is delivered to a point at the depth of maximum dose in a water-equivalent phantom placed at 100 cm of the x-ray source, with a field size of 10×10 cm^2 at the surface [1]. The detector was placed at a depth $z = 10$ cm. Let us denote by M_Q^* the charge read by the electrometer (in nC) for a beam of quality Q (6 or 15 MV); "quality" refers to an index that quantifies the penetration of a photon beam. First we convert the electrometer reading to the reference pressure P_0 and temperature T_0 at the Dosimetry Standards Laboratory where the dosimeter was calibrated,

$$M_Q = M_Q^* \, k_{TP} \tag{1}$$

*Electronic address: suen1996@gmail.com

with

$$k_{\mathrm{PT}} = \frac{(273.2\ \mathrm{K} + T)P_0}{(273.2\ \mathrm{K} + T_0)P}, \tag{2}$$

being P and T the pressure and temperature during the measurement at the hospital [1]; our ionization chamber was calibrated at the Ciemat (Madrid) so that $P_0 =$ 760 mmHg and $T_0 = 20°\mathrm{C}$. Then, the absorbed dose is determined from the product

$$D_{\mathrm{w}} = M_Q\, N_{D,\mathrm{w},Q_0}\, k_{Q,Q_0} \prod_i k_i, \tag{3}$$

where N_{D,w,Q_0} (in cGy/nC) is the calibration coefficient for the reference quality Q_0 employed to calibrate the dosimeter at the Dosimetry Standards Laboratory (^{60}Co at the Ciemat) and k_{Q,Q_0} is the beam quality correction factor. Finally,

$$\prod_i k_i = k_{\mathrm{s}}\, k_{\mathrm{pol}}, \tag{4}$$

where k_{s} and k_{pol} are the recombination and polarization correction factors. k_{s} corrects the response of an ionization chamber for the lack of complete charge collection due to ion recombination. Its expression is

$$k_{\mathrm{s}} = a_0 + a_1\,(M_1/M_2) + a_2\,(M_1/M_2)^2\,, \tag{5}$$

where M_1 and M_2 are the readings obtained for voltages V_1 and V_2. M_2 is the value for the smallest voltage at absolute value. For a pulsed beam and $V_1/V_2 = 4.0$ the parameters are $a_0 = 1.022$, $a_1 = -0.363$, $a_2 = 0.341$. In turn, k_{pol} corrects the response of an ionization chamber for the effect of a change in polarity of the polarizing voltage applied to the chamber,

$$k_{\mathrm{pol}} = \frac{|M_+| + |M_-|}{2M}, \tag{6}$$

being M_+ and M_- the measurements for two opposite potentials, and M the electrometer reading obtained with the polarity used routinely (-200 V in our case) [1, 2]. For the cylindrical chamber, these correction factors had been determined at the hospital with multiple measurements during different days and are collected in Table I.

TABLE I: Correction factors for the PTW-30013 ionization chamber. Their uncertainty is 1.5%.

Q	k_{Q,Q_0}	k_{s}	k_{pol}
6 MV	0.992	1.002	1.000
15 MV	0.975	1.004	1.000

To determine the absorbed dose inside the bone and lung slabs we employed a NACP02 plane-parallel ionization chamber because we did not have a bone insert slab for the cylindrical chamber. We used three phantoms of 30 cm $\times$ 30 cm consisting of top and bottom layers made of plastic water and a middle layer made of either plastic water, lung or bone, Fig.(1). We used a 100 MU and the detector was placed at a depth of 8 cm.

As we did not have the calibration coefficient for the plane-parallel chamber we had to cross-calibrate it at the hospital with the factor we already had for the cylindrical chamber and additional measurements that were carried out with a plastic water phantom and a detector at $z =$ 10 cm. We also had to calculate the recombination and polarization factors with Eqs. (5) and (6).

B. Treatment-planning systems

The calculations were done with the Eclipse Treatment System (Varian Medical Systems) which has incorporated the AAA and Acuros v.13.5.35 algorithms.

Convolution-superposition models are based on the overlay of different integrations in different materials having determined previously a point kernel for each material. A kernel is the distribution of the dispersed radiation around an ideal point of interaction which is then integrated with the fluence of the primary photons.

AAA is a model of this type but quite simple. It modifies the shape of a water kernel based on the mass density of the calculation points, in the three main directions of space. Problems appear around heterogeneities because the spatial discretization is too coarse and for materials such as bone, for which the water kernel re-scaled with the bone density is not a good approximation.

Recently, new algorithms based on the solution of the linear Boltzmann transport equation (LBTE) have been developed. The LBTE describes the transport (i.e. propagation and interaction) of charged and neutral particles in a medium. There are two techniques that can be used to solve it numerically:

1. Stochastic Monte Carlo method: the expected value of the dose is estimated by the average of a large number of random showers of primary and secondary particles. Although it has a simple implementation, it is very time-consuming.

2. Deterministic methods: the particle's transport is discretized in phase space, energy is also discretized and the spatial discretization is carried out using an adaptive mesh. Advantages of this method are that material heterogeneities are considered as each voxel is designated a different material property with its cross sections, it is free from statistical noise and it is around 2 to 4 times faster than Monte Carlo simulation.

Acuros is the latest version of this family of algorithms. It solves the LBTE with a sophisticated technique and accounts for the effects of heterogeneities made of materials such as lung, bone, air and non-biological implants, may have on patient dose calculations [3, 4].

C. Monte Carlo simulations

PENELOPE is a code system for the Monte Carlo simulation of coupled electron-photon transport in homogeneous materials for a wide range of energies, 50 eV to 1 GeV [5]. It allows an accurate simulation of the radiation beams delivered by a linac, describing in detail its geometry and applying elaborate variance-reduction techniques to achieve low statistical uncertainties in a reasonable computing time [6].

In order to run a simulation with PENELOPE/penEasy we had to create several files.

a. Geometry The PENGEOM package was used to model the different phantoms. PENGEOM describes geometries by means of quadric surfaces. We started from the subset of "canonical" quadrics, defined by the equation

$$F_{\rm r}(\vec{\mathbf{r}}) = I_1 x^2 + I_2 y^2 + I_3 z^2 + I_4 z + I_5, \qquad (7)$$

where $I_i = +1, 0, -1$ for $i = 1, \ldots, 5$. If necessary, the canonical quadrics were scaled, rotated and translated to generate arbitrary quadrics. Each surface defines two regions that are identified by the surface Side Pointer (SP). If $F(\vec{\mathbf{r}}) < 0$ (SP$= -1$), a point $\vec{\mathbf{r}} = (x, y, z)$ is said to be "inside" the surface, while if $F(\vec{\mathbf{r}}) > 0$ (SP$= +1$) the point is regarded to be "outside" [5].

The next step was to create the bodies which are determined by limiting surfaces. It is convenient to define the bodies in an ascending order to avoid possible overlaps. Thus, for a complex geometry, first we would define the innermost bodies and then the rest of them would be delimited by their surfaces and the previously-defined bodies.

The geometries were constructed with 13 surfaces and 5 bodies. They consist of a $30 \times 30 \times 15$ cm^3 phantom made by three 5-cm-thick layers and a scoring volume ("dosimeter") of $4 \times 4 \times 0.1$ cm^3 placed at a depth of 8 cm on the z axis. The beam was simulated as a square field on the surface of 10×10 cm^2 and 0.1 cm thick.

b. Materials The material data files were created by the auxiliary program MATERIAL. The chemical composition and the mass density of each material were entered manually as they did not appear in PENELOPE's database [7].

The top and bottom layers, as well as the square field on the surface, were made by plastic water. The middle slab was made by bone or Saint Bartholomew's lung, whose compositions were provided by the hospital. The "dosimeter" was a cavity of liquid water, bone or lung depending on whether we were calculating dose to water or dose to medium.

c. Input file This is the configuration file needed by the main program penEasy [6] to run the simulation. Its different sections characterize the details of our simulation: type of particles, initial position and size of the source, particle's direction and energy, the geometry and materials used, etc. The number of simulated primary particles was always 10^8 in order to have good statistics ($\leq 0.3\%$). The energy distribution of the photons was introduced by two energy spectrum files, Varian 6 MV and Varian 15 MV [8]. The adopted spectra lack the component of low-energy electron contamination. To simulate it we would have needed phase-space files for the linac.

The input file allows the activation of various tallies to obtain the desired information. We activated the tally of Energy Deposition that created a file with the energy deposited (eV/history) in each body.

Three types of variance-reduction techniques can be applied to reduce the simulation time considerably; we activated the first one, interaction forcing. This technique increases the interaction probability by artificially increasing the interaction cross sections. In this way, while the average of the deposited energy is unbiased, the variance is reduced by a factor equal to the forcing factor [7]. In our simulations, we have forced Compton interactions inside the detector by a factor of 100.

D. Conversion $D_{\rm w}$ - $D_{\rm m}$

To determine the absorbed dose to water, $D_{\rm w}$, at a point P inside a medium m we use the Bragg–Gray cavity theory. It simulates a small cavity full of water around P which must not disturb the fluence distribution (energy spectrum) of charged particles $(\Phi_E)_{\rm m}$ existing in the absence of the cavity. The absorbed dose to water, $D_{\rm w}$, and absorbed dose to medium, $D_{\rm m}$, are connected through the equation

$$D_{\rm w} = D_{\rm m}\, s_{\rm w,m} \qquad (8)$$

with the so-called Bragg–Gray stopping-power ratio

$$s_{\rm w,m} \equiv \frac{\int_0^{E_{\max}} (\Phi_E)_{\rm m}\, (S_{\rm el}/\rho)_{\rm w}\, {\rm d}E}{\int_0^{E_{\max}} (\Phi_E)_{\rm m}\, (S_{\rm el}/\rho)_{\rm m}\, {\rm d}E}; \qquad (9)$$

here $S_{\rm el}/\rho$ is the mass electronic stopping power [9]. AAA only reports $D_{\rm w}$ whereas Acuros can provide either $D_{\rm w}$ or $D_{\rm m}$.

III. RESULTS AND DISCUSSIONS

The doses under reference conditions for the day of the measurements, calculated with Eq. (3), were $D_{\rm day}(6\ {\rm MV}) = 0.709(19)$ Gy and $D_{\rm day}(15\ {\rm MV}) = 0.822(20)$ Gy. For this project, all the quoted uncertainties correspond to 1 SD.

We have employed the calibration coefficient for the cylindrical chamber, $N_{D,{\rm w},Q_0} = 5.396(30)$ cGy/nC, the correction factor for pressure and temperature calculated with Eq. (2), where $P = 760.1$ mmHg and $T = 24.3$°C,

that is $k_{PT} = 1.0145(9)$, and the correction factors from Table I.

The rest of the measurements were done with the NACP02 plane-parallel ionization chamber. As we did not have its calibration coefficients, we calculated them by doing a cross-calibration at the hospital,

$$N_{D,\mathrm{w},Q} = \frac{D_{\mathrm{day}}}{M_{Q,\mathrm{cyl}}} \frac{1}{\prod_i k_i}. \tag{10}$$

This equation yields $N_{D,\mathrm{w},Q}(6\ \mathrm{MV}) = 0.164(4)$ Gy/nC and $N_{D,\mathrm{w},Q}(15\ \mathrm{MV}) = 0.159(4)$ Gy/nC. Previously, we had calculated the correction factors for this chamber using Eqs. (5) and (6); the values are collected in Table II.

TABLE II: Correction factors for the NACP02 chamber.

Q	k_{s}	k_{pol}
6 MV	1.0047(1)	0.9974(1)
15 MV	1.0084(1)	0.9981(1)

The dose of the day under reference conditions fluctuates with respect to the reference dose that Eclipse has incorporated from the day it was configured. The experimental doses of Table III were thus corrected with all the correction factors and with the reference dose, using equation

$$D_{\mathrm{w}} = \bar{M}_Q\, N_{D,\mathrm{w},Q} \left(\prod_i k_i \right) D_{\mathrm{ref}}/D_{\mathrm{day}}. \tag{11}$$

TABLE III: Doses corrected with the dose of the day and the correction factors of the NACP02 chamber.

	D_{w} (Gy)	
Material	6 MV	15 MV
Water	0.7865(8)	0.8933(13)
Lung	0.8229(8)	0.9194(4)
Bone	0.7312(20)	0.8696(3)

The calculations done with AAA and Acuros are found in Table IV, which also contains in the last column the values of D_{w} calculated by means of Eq. (8) and $s_{\mathrm{w,m}}$ from ref. [9]. The deviations between calculations and measurements, Table V, have been reported as

$$\delta = 100\,(D_{\mathrm{calc}} - D_{\mathrm{meas}})/D_{\mathrm{meas}}. \tag{12}$$

These results showed that differences between measures and calculations with Acuros have decreased in comparison with AAA. However, in the case of bone, differences were extremely larger than 2%. The reason why this happened was that ionization chambers are calibrated inside a water phantom, they are not prepared to be used inside a slab of bone or lung. However, in the case of lung, the results seem to be quite good because lung is more similar in composition to water (different mass density and different scattering) than bone, which has a very different composition, with a higher component of the photoelectric effect compared to the Compton effect.

TABLE IV: Absorbed doses (in Gy) calculated with AAA and Acuros.

	Material	AAA	Acuros, D_{w}	Acuros, D_{m}	D_{w}
6 MV	Water	0.776	0.773	0.773	–
	Lung	0.783	0.805	0.803	0.811
	Bone	0.777	0.826	0.745	0.848
15 MV	Water	0.881	0.879	0.879	–
	Lung	0.895	0.902	0.911	0.920
	Bone	0.877	0.958	0.864	0.979

TABLE V: Deviations (in %) between measurements and calculations with AAA and Acuros.

	Material	AAA	Acuros, D_{w}	Acuros, D_{m}	D_{w}
6 MV	Water	1.3	1.7	1.7	–
	Lung	4.9	2.2	–	1.4
	Bone	6.3	13.0	–	15.9
15 MV	Water	1.4	1.6	1.6	–
	Lung	2.7	1.9	–	0.1
	Bone	0.9	10.2	–	12.6

Introducing a finite cavity of a material medium inside another material medium can cause a perturbation of the particle fluence. Consequently, the ratio between the measured D_{w} and the value calculated according to Eq. (8), will differ from 1. The perturbation factor was then calculated as $P_{\mathrm{per}} = D_{\mathrm{m}}/D_{\mathrm{w}}$. These values were obtained by simulating the inner cavity of our detector, a cylinder 2 mm high and 5 mm of radius, made of bone to obtain D_{m} and of water to obtain D_{w}. This last value was converted to D_{m} by using the stopping power ratio of bone. The results were $P_{\mathrm{per}}(6\ \mathrm{MV}) = 1.116(2)$ and $P_{\mathrm{per}}(15\ \mathrm{MV}) = 1.113(3)$. Table VI contains the measurements corrected with these factors. In this way, differences between calculation and experiment decreased notably to around 2%, see Table VII.

TABLE VI: Experimental absorbed doses at $z = 8$ cm inside the slab of bone corrected with the perturbation factors.

	D_{w}(Gy)	
Material	6 MV	15 MV
Bone	0.819(3)	0.965(3)

Table VIII contains the predictions of Monte Carlo simulations. The absorbed doses to water, D_{w}, obtained with MC should match with the experimental measurements. We have plotted the depth-dose profiles in Figs. 2 and 3, where we can see that the results match as expected. However, all the experimental points are slightly below the D_{w} curves.

TABLE VII: New differences (in %) between the experimental absorbed dose and the calculations.

	Material	AAA	Acuros, D_w	Acuros, D_m	D_w
6 MV	Bone	5.1	0.9	–	3.5
15 MV	Bone	9.1	0.7	–	1.4

TABLE VIII: Absorbed doses at $z = 8$ cm for the phantoms simulated with PENELOPE/penEasy.

	D_w(keV/hist)		D_m(keV/hist)	
Material	6 MV	15 MV	6 MV	15 MV
Water	2.960(7)	5.504(10)	2.960(7)	5.498(10)
Lung	2.853(7)	4.709(9)	0.798(3)	1.329(3)
Bone	2.825(7)	5.713(11)	5.112(11)	10.22(2)

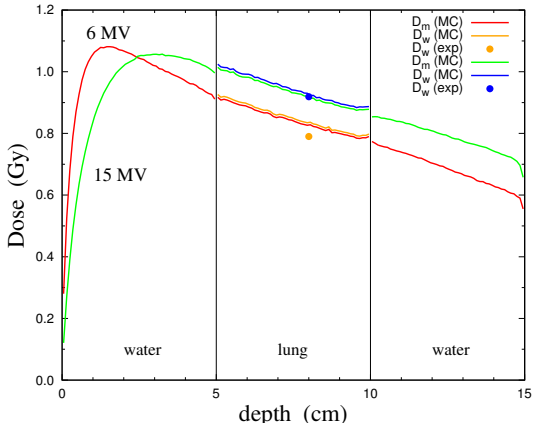

FIG. 2: Depth-dose profiles simulated with PENELOPE (continuous lines) and the experimental measurements (points) for lung. The error bars are smaller than the size of the symbol.

IV. CONCLUSIONS

The absorbed doses calculated with the algorithm of Acuros agreed better, with differences around 2%, with the experimental data measured with the ionization chamber than the values calculated with the algorithm implemented in AAA. Therefore, Acuros represents an improvement over AAA. However, at lower energies, where the scatter dose is of greater importance than the primary dose, differences were still high. New approaches should emerge to achieve better results.

In addition, the experimental data and the simulated values for the absorbed dose do also agree as it has been seen in Figs. 2 and 3.

The energy spectra adopted in the simulations contained only x-rays, but did not have electron or positron contamination. In order to improve this project, the whole gantry of the linac could be simulated to model the beams more realistically.

Furthermore, it should be contemplated the possibility of using other detectors, e.g. ultrathin thermoluminiscent detectors which cause a negligible perturbation.

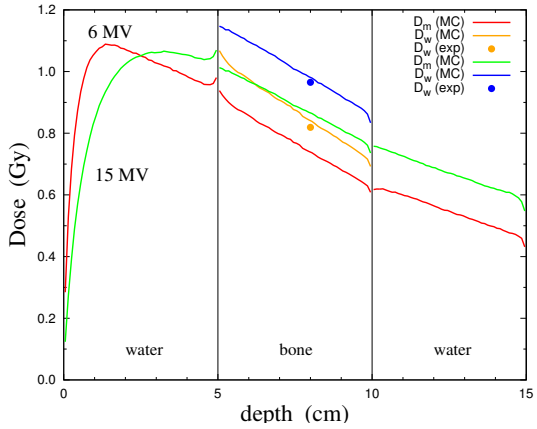

FIG. 3: Depth-dose profiles simulated with PENELOPE (continuous lines) and the experimental measurements (points) for bone. The error bars are smaller than the size of the symbol.

Acknowledgments

I would like to thank my advisor Dr. J. M. Fernández-Varea for guiding and supervising this project. I appreciate the help and support I received from the radiophysics team of Hospital de la Santa Creu i Sant Pau during my stay there. In particular, the support by Dr. Pablo Carrasco was very valuable. Finally, I thank my family and friends for their encouragement throughout this period.

[1] Mayles, P., Nahum, A. and Rosenwald, J.C., *Handbook of Radiotherapy Physics* (Taylor & Francis, 2007).
[2] IAEA TRS-398, v.12, 2006.
[3] Jiankui, Y., Jette, D. and Chen,W., Med. Phys. **35** (2008) 4079.
[4] A. Failla, G., Wareing, T., Archambault, Y. and Thompson, S., *Acuros XB advanced dose calculation for the Eclipse treatment planning system*. Varian Medical Systems.
[5] Salvat, F., La Cité des Sciences et de lIndustrie, Paris, France, (2013).
[6] Sempau, J., Badal, A. and Brualla, L., Med. Phys. **38** (2011) 5887.
[7] Salvat, F. "Penelope-2014. A Code System for Monte Carlo Simulation of Electron and Photon Transport" (OECD/NEA, Issy-les-Moulineaux, 2015).
[8] Sheikh-Bagheri, D. and Rogers, D. W. O., Med. Phys. **29** (2002) 391.
[9] Fernández-Varea, J.M., Carrasco, P., Panettieri V. and Brualla, L., Phys. Med. Biol. **52** (2007) 6475.